CARMINIC ACID INCORPORATED INTO SPHERICAL CELLULOSE NANOPARTICLES. THEIR PREPARATION AND CHARACTERIZATION

NELLY FLORES-RAMÍREZ,[*] ALIA NOHEMÍ YHAMEL-GARCÍA,[*] SALOMÓN R. VÁSQUEZ-GARCÍA,[*] HÉCTOR MARTÍNEZ FLORES,[*] LADA DOMRATCHEVA-LVOVA[*] and LEANDRO GARCÍA-GONZÁLEZ[**]

[*]*Michoacan University of Saint Nicholas of Hidalgo, Morelia, Mich. 58060, México*
[**]*Micro and Nanotechnology Research Center, Boca del Rio, Veracruz, 94292, México*
✉ *Corresponding author: Nelly Flores-Ramírez, frnelly@umich.mx*

Received October 31, 2016

Carminic acid (CA) was added by two processes: dipping or *in situ*, to cellulose nanoparticles previously obtained using Span 80 and 85 as emulsifiers. The resulting nanoparticles were analyzed by Scanning Electron Microscopy (SEM), Atomic Force Microscopy (AFM) and Fourier Transform Infrared (FTIR) spectroscopy. According to both SEM and AFM studies, the pure cellulose nanoparticles showed spherical geometry with an average diameter in the range of 150-400 nm. At concentrations of 0.2 and 0.5 wt% of CA, the cellulose nanoparticles increased their average diameter and aggregation state. It was observed that the cellulose nanoparticles absorbed CA, which was spotted to be higher when using the *in situ* process, compared to the dipping process. However, with the dipping process, the spherical geometry of the nanoparticles was maintained after CA absorption, resulting in a significant increase in their diameters from 150-400 nm to 900 nm. The molecular associations between nanoparticles and CA were determined by FTIR studies, which revealed that an increase of the absorbance ratio occurred upon the addition of CA. Thus, in this work, the process of CA absorption was established, which opens a new perspective for the fabrication of a safety indicator in packaged foods, where CA could serve as a new sensor to measure the quality of food.

Keywords: cellulose, carminic acid, nanoparticles, inverse emulsion, dipping and *in situ* processes

INTRODUCTION

High standards of food safety and hygiene are essential to reduce the risk of food poisoning. Nanotechnology is a solution to this problem, whether packages include nanomaterials or nanoparticles, since these can respond to environmental conditions and alert consumers about potential contamination of food by the presence of pathogens and toxins. Furthermore, nanoparticles exhibit different physical and chemical properties for a large number of uses and applications.[1-4] For instance, nanoparticles are considered as "smart" materials when they are used as a "nanosensor" for detecting microbial contaminants.[5-7] Nanosensors can increase the flexibility and scope of quality control tests, directly related to the product. This is suitable in the food industry since nanodevices present specificity, selectivity and adaptability.[8,9]

Carminic acid (CA) is an organic molecule used as nanosensor, it is a natural dye, which is required by the food, cosmetic and pharmaceutical industries.[10-12] Meanwhile, cellulose is by far the most widely used biopolymer matrix for dyes, due to its absorption, lightness and degradability characteristics. Basically, cellulose is a polysaccharide formed by large glucose chains, which is not water-soluble because of its bonds and the interactions of hydrogen with the glucose chains. Cellulose structure presents crystalline and amorphous regions, which allows the formation of micelles.[13,14] By controlling its microstructure, the physical and chemical properties of cellulose can be modified in any manner desired. Thus, recently, some authors have reported the preparation of cellulose nanoparticles with spherical geometries with diameters of several hundred nanometers to serve as matrix.[15] Some of them have been prepared by acid hydrolysis of cellulosic fibers or from short staple cotton by pre-swelling the fibers, prior to acid hydrolysis.[16-22]

Based on the above-mentioned considerations, in this research, an inverse emulsion was used to obtain cellulose nanoparticles containing CA, so that they could act as a safety indicator or nanosensor

in packaged foods. The obtained nanoparticles could be incorporated into stickers, which can be preferably adhered to a semi-permeable surface of a food-packaging film. This sticker would change its color, depending on the period of time and the temperature at which the product has been stored, thus providing consumers with much more information about the quality of a particular product.

EXPERIMENTAL

Reagents

All solvents and reagents used in the study were purchased from Sigma-Aldrich Co.: sulphuric acid (H_2SO_4), hydrochloric acid (HCl), sodium hydroxide (NaOH), hexane and acetone. SPAM 80 and 85 were used as emulsifiers. CA with a molecular weight of Mw = 492.39 g/mol was used without pretreatment.

Obtainment of cellulose

The Kraft pulping process was used to obtain bleached wood pulp from 17-20 year old *Eucalyptus saligna* wood. At first, an alkali pretreatment was performed by cooking industrial-size wood chips (10.2 x 5.1 x 5.1 cm) at a liquor-wood ratio of 1:4 (w/v), followed by a drying process. After that, the dried chips were treated in a 5000 mL Parr reactor. The liquor composition was 82% active alkali and 23.8% sulfidity (both calculated on a dry wood basis and expressed as Na_2O equivalents). The loaded reactor was heated from 20 °C to 120 °C, with a rate of 1.6 °C/min and keeping this temperature for 30 min. After this time, the temperature was increased and kept at 155 °C for 30 min. Finally, the reactor temperature was raised to 160 °C for 2 h. After cooking, the pulps were disintegrated in a TAPPI laboratory blender, thoroughly rinsed with tap water, and centrifuged. For bleaching the pulp, chlorine dioxide, alkaline extraction, hypochlorite, and peroxide treatment were used.

Preparation of the cellulose nanoparticles

The cellulose nanoparticles were prepared *via* an inverse emulsion method using hexane as continuous phase (Fig. 1). First, a continuous non-polar phase was prepared by pouring 100 mL of hexane, containing 0.5 g of SPAN 80 and 85, into a glass reactor equipped with a Compact Digital Stirrer BDC 2002. Second, the discontinuous phase was prepared by dissolving 0.5 g of cellulose in an acid solution (comprising 70% w/w of HCl). Afterwards, the discontinuous phase was added into the continuous phase; the third step consisted in heating the solution at 55±2 °C for 3 h at a stirring rate of 600 rpm. Finally, the emulsion obtained was centrifuged in a refrigerated centrifuge (Hermile brand model Z400K) and the fractions were then rinsed repeatedly with acetone.

Incorporation of CA into the cellulose nanoparticles

The dipping and *in situ* incorporation processes were performed by using two different concentrations of CA. In both processes, 200 (0.2 wt%) and 500 (0.5 wt%) mg of CA were dissolved in 1 L of distilled water and kept under magnetic stirring for 20 min at room temperature. For the dipping process, there was a special consideration: the above solutions contained 30 mL of additional acetone. Also, in the dipping process, the CA solutions were under magnetic stirring at room temperature when the cellulose nanoparticles were added; after this addition, the solution was kept under the same conditions for 20 min. Meanwhile, for the *in situ* process, the CA solutions were added to the cellulose solution.

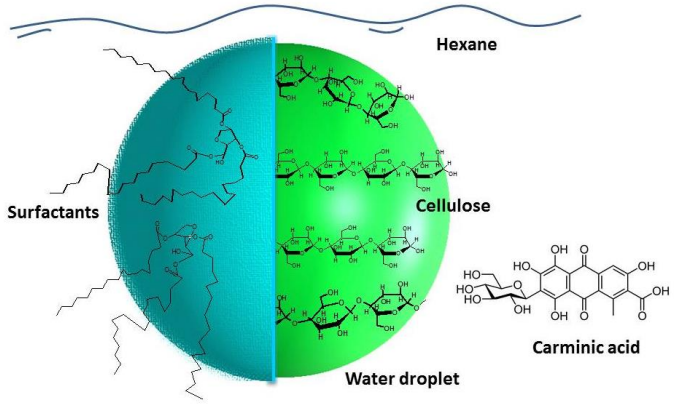

Figure 1: Schematic representation of cellulose chains in the hexane phase (inverse emulsion) and carminic acid

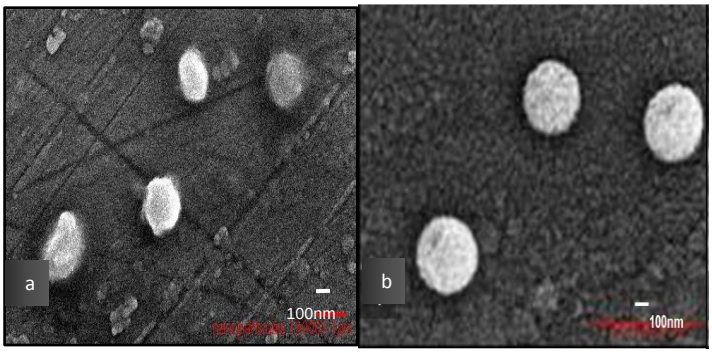

Figure 2: SEM images of pure cellulose nanoparticles on glass substrates a) at 10,000x and b) at 60,000x

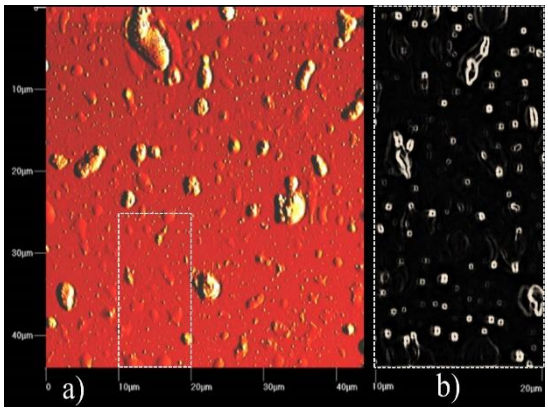

Figure 3: AFM images of pure cellulose nanoparticles on glass substrates; a) nanoparticles and aggregates; b) a magnified selected area

Methods of characterization

The nanoparticles were characterized using a JEOL JSM 5300 Emission Scanning Electron Microscope (SEM). Prior to the SEM analysis, all the samples were coated with graphite. The morphological characteristics of the nanoparticles were obtained using Atomic Force Microscopy (AFM). The AFM used was an Olympus model IX-70 (Olympus America, Melville, N.Y.) with a rate of 0.2 Hz. Fourier Transform Infrared Spectroscopy (FTIR) was obtained using a Tensor 27 Bruker spectrometer in the 2000-400 cm^{-1} spectral range at a resolution of 4 cm^{-1} in the absorption mode. All nanoparticles were analyzed without further treatment.

RESULTS AND DISCUSSION

Morphological characterization

Figure 2 (a and b) shows SEM images of the pure cellulose nanoparticles with magnifications of 10,000X and 60,000X, respectively. The SEM images show nanoparticles dispersed on a glass surface with spherical geometries with an average diameter of 150 to 400 nm.

Figure 3 shows AFM images of pure cellulose nanoparticles. Figure 3a presents some agglomerates with diameters of 1 to 10 µm. Also, a discrete area (marked with dashed lines) may be noted in this image, which was selected with the purpose of visualizing with sufficient detail some individual nanoparticles. This area was amplified and adjusted to black and white with an edge lighting effect (Fig. 3b). In this way, the nanoparticles revealed a round shape with an average diameter of 150 to 250 nm.

Both SEM and AFM images show nanoparticles, which can be defined as nanospheres with a size distribution from 150 to 400 nm. The size and range in size of these nanospheres indicate that the method of processing the nanospheres is favorable within certain size parameters. By contrast, it is reasonable to assume that some of these nanoparticles were joined by aggregation and agglomeration mechanisms during the nanosphere formation process.

Figure 4 shows SEM images of cellulose nanoparticles in the presence of CA, obtained by the dipping process. Figure 4a reveals cellulose nanoparticles at 5,000X magnification, resulting from the use of the solution of 200 mg/L (0.2 wt%) of CA. From the image, it may be noted that nanoparticles formed aggregates of micron sizes, which were surrounded by CA. Additionally, it was estimated that

the particles displayed sizes above 900 nm. The estimated average nanoparticle size was obtained by measuring the cross-sectional areas of at least ten particles; one of them is shown in Figure 4. The increase in the diameter of the nanoparticles reveals a positive interaction between CA and cellulose nanoparticles, because the particles of cellulose were fully coated and embedded in the CA. The cellulose nanoparticles absorbed the CA, thus the sizes of the cellulose nanoparticles were increased. It suggests that there was a good compatibility between CA and the nanoparticle matrix. This result can be explained by the fact that both CA and cellulose molecules contain multiple hydroxyl groups in their molecular structures, which interact through hydrogen bonding to form a three-dimensional structure.

As may be remarked in Figure 4b (6,000X), after increasing the CA concentration from 0.2 to 0.5 wt%, the aggregations of nanoparticles were maintained, but the agglomerate did not have a definite geometry. The nanoparticles only had regular geometry at a concentration of 0.2 wt% of CA, because at higher concentration, they were saturated with the CA solution.

Figure 5 shows SEM images of cellulose nanoparticles obtained by the *in situ* process at two CA concentrations, 0.2 and 0.5 wt%. Figure 5a illustrates the effect of the 0.2 wt% CA solution on the nanoparticles. This concentration led to the formation of irregularly shaped particles with a size of around 3 μm, within which, the presence of embedded particles can be observed, with dimensions that could not be measured in this study because their edges were not well-defined.

Figure 5b clearly illustrates that when the CA concentration is increased to 0.5 wt%, the CA has a heterogeneous surface, and the cellulose particles are located on and within the matrix. To visualize the morphology of these cellulose particles in more detail, Figure 5c presents a zoom-in view of Figure 5b. From this image, oval nanoparticles with diameters from 300 to 500 nm are observed. Further analysis indicated that some nanoparticles dissolved into the CA.

A comparison of the CA-containing nanoparticles obtained by dipping and by the *in situ* process led to the conclusion that the first appeared to be more resistant to the CA solutions than the latter. This was based on the performance of the nanoparticles: the first showed agglomerations, while the latter presented poor dimensional stability, indicating that the CA could be completely integrated into cellulose. These differences can be explained by nanoparticle formation. The inverse emulsion process yielded spherical deformable nanoparticles, which were hardened by the acidic treatment. This was related to the relatively high density and the correspondingly low porosity of the nanoparticles, that is, the nanoparticles subjected to the dipping process were relatively resistant to swelling and deformation in aqueous or organic solutions. This property contrasted with that of the nanoparticles obtained by the *in situ* process.[19]

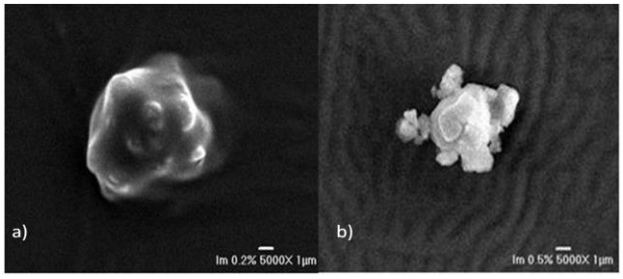

Figure 4: SEM images of cellulose nanoparticles with CA added by dipping, a) 0.2 wt% CA and b) 0.5 wt% CA

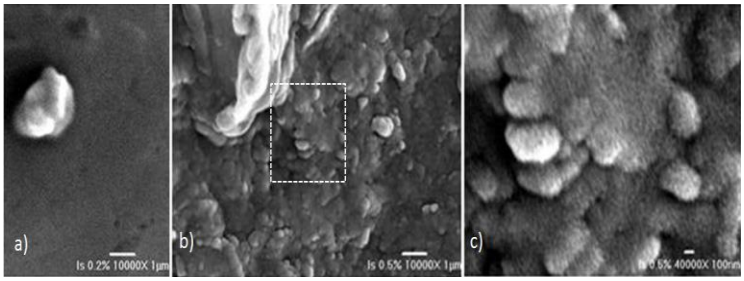

Figure 5: SEM analysis of cellulose nanoparticles with CA added *in situ*, a) 0.2 wt% CA, b) 0.5 wt% CA and c) zoom-in view of the square region

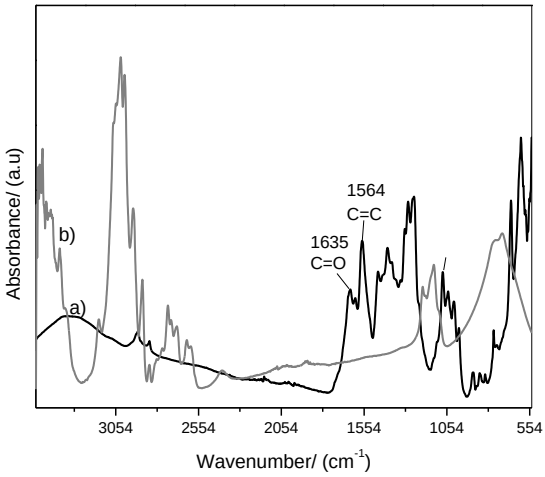

Figure 6: FTIR spectra of a) CA and b) pure cellulose nanoparticles

FTIR spectroscopy

Figure 6 presents the FTIR spectra of the pure CA (a) and of the cellulose nanoparticles (b). The spectrum in Figure 6a presents the stretching vibration due to the OH groups at 3335 cm^{-1}. The presence of the hydrocarbon chain can be identified at 2925 and 2844 cm^{-1}, corresponding to the vibration of CH_3 and CH_2, respectively. Additionally, the two signals at 1635 and 1564 cm^{-1} can be ascribed to the C=O and C=C groups. Finally, the OH and C-OH groups are identified by the deformation and stretching vibration at 1289 and 1081 cm^{-1}, respectively.[10-23]

The FTIR spectrum of the cellulose nanoparticles (Fig. 6b) presents a symmetric stretching vibration at 3495 cm^{-1}, which is characteristic of –OH groups. Stretching vibrations of CH and CH_2 group are found at 2917 and 2853 cm^{-1}, respectively. The asymmetric stretching vibration of the C-O-C bonds of glucose units can be noted at 1163 cm^{-1}. Additionally, at 1105 cm^{-1}, a band corresponding to the asymmetric stretching of the glucose ring is observed. Finally, at 1054 and 1028 cm^{-1}, the symmetric stretching vibrations of C-O bonds are present.[24] Compared with cellulose, the cellulose nanoparticles did not show any new signals.

The FTIR spectra recorded for the cellulose nanoparticles obtained with four CA concentrations (0.05, 0.10, 0.20 and 0.50 wt%) by the dipping process are illustrated in Figure 7. The 0.10 and 0.20 wt% CA-containing cellulose nanoparticles showed the highest absorption bands, indicating that the CA was more efficiently absorbed at these concentrations. The absorption bands decreased with an additional increment in the amount of CA (0.50 wt%), indicating that the surface of the cellulose nanoparticles was already saturated at lower CA concentrations. Particularly, the band related to OH stretching was more prominent for the two intermediate concentrations (0.10 and 0.20 wt%) than for the two extreme concentrations (0.05 and 0.50 wt%). It could be due to the limited number of hydroxyl groups that can be associated to the cellulose through their polar groups. The OH and C=O stretching bands observed at 3500-3000 cm^{-1} and 1750-1400 cm^{-1}, respectively, did not show any shift by decreasing the CA concentration. It indicates that there were no interactions among the polar groups.[25]

Figure 8 shows the FTIR spectra of the CA-containing cellulose nanoparticles obtained by the *in situ* process, for four different CA concentrations. From the spectra, it can be observed that the absorption signals increase as the CA concentration is increased. Thus, the cellulose nanoparticles were able to absorb a high amount of CA. Figure 8b shows the spectral region between 1700-1400 cm^{-1}. The main signals did not present any shift in response to the increase of the CA concentration, but did show an increase in absorbance.

The difference between the two types of nanoparticles (obtained by the dipping and *in situ* processes) consists in the fact that the nanoparticles dipped into CA were able to absorb a limited amount of CA and presented a saturation level around 0.1-0.2 wt% (Fig. 7a). In contrast, the nanoparticles with *in situ* incorporated CA reached a higher amount of CA (Fig. 8).

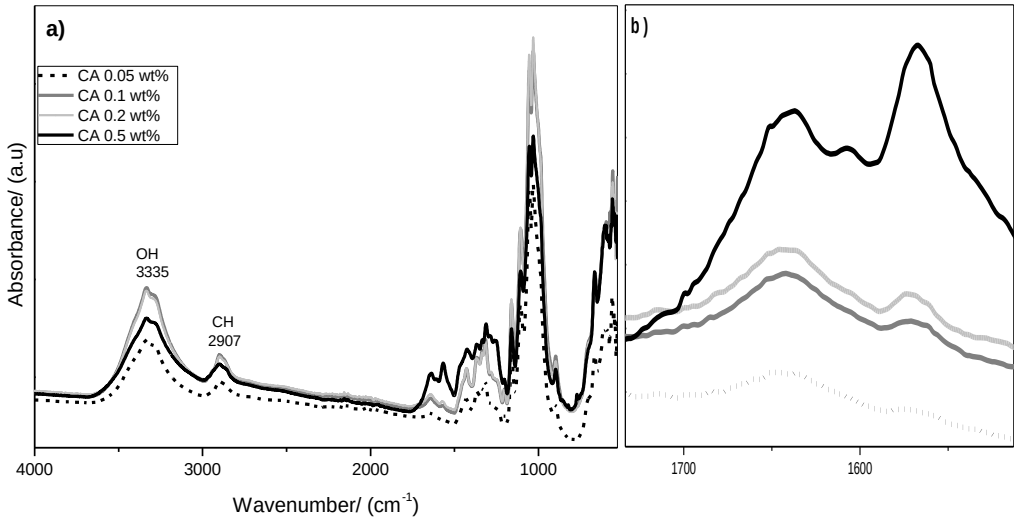

Figure 7: FTIR spectra of CA-containing cellulose nanoparticles obtained by dipping at different CA concentrations, a) full view of the spectra and b) zoom-in of the region between 1750-1400 cm^{-1}

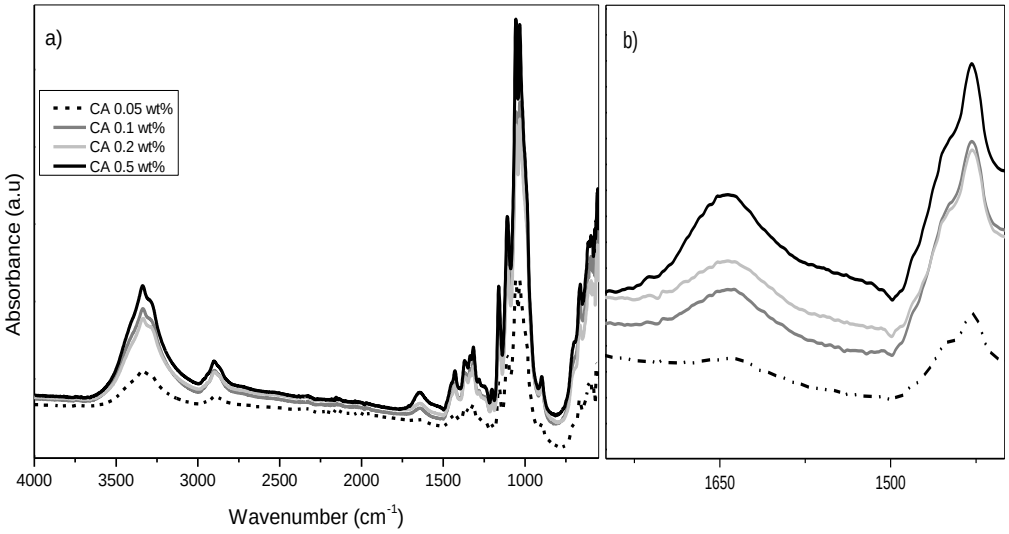

Figure 8: FTIR spectra of CA-containing cellulose nanoparticles obtained *in situ* at different CA concentrations, a) full view of the spectra b) zoom-in of the region between 1700-1400 cm^{-1}

CONCLUSION

The present work achieved nanometric spherical cellulose particles, with sizes between 150 to 400 nm, synthesized by the inverse emulsion procedure. CA was successfully incorporated into the cellulose nanoparticles by the dipping and *in situ* processes, and some differences between the obtained CA-containing nanoparticles were revealed. The nanoparticles subjected to the dipping process were saturated with low amounts of CA (less than 0.2 wt%) and had dimensions around 900 nm. However, when the CA was added *in situ*, amorphous particles around 3 µm were formed, which absorbed more CA, increasing the degree of dissociation of the particles. The results of the investigation were in agreement with the FTIR analysis of the nanoparticles, which revealed that the main functional groups of CA increased the absorbance ratio as the CA concentration was increased, which had a low limit for the addition of CA by dipping. Finally, the spherical geometry of the CA-containing nanoparticles was preserved when the dipping process was applied.

ACKNOWLEDGEMENTS: The authors are thankful for the financial support from PROMEP Collaborative Thematic Networks. Coordination of Scientific Research (UMSNH) and National Council of Science and Technology (CONACyT-Mexico) under the projects approved No. 104259,

61414 are acknowledged. The authors are also very grateful to Ma Remedios Cisneros Magaña (from IIM-UMSNH).

REFERENCES

[1] A. L. Brody, B. Bugusu, J. H. Han, C. K. Sand and T. H. McHugh, *J. Food Sci*., **73**, R107 (2008).
[2] J. Lee and Y. Deng, *Soft Matter*, **7**, 6034 (2011).
[3] V. M. Granda, G. A. C. Valdés, C. J. A. García and M. E. Díaz-Garcia, *Microchim. Acta*, **166**, 1 (2009).
[4] D. A. Pereira de Abreu, J. M. Cruz and P. Paseiro Losada, *Food Rev. Int*., **28**, 146 (2012).
[5] T. V. Duncan, *J. Colloid Interface Sci*., **363**, 1 (2011).
[6] G. I. Olivas and G. V. Barbosa-Canovas, *Crit. Rev. Food Sci*., **45**, 657 (2005).
[7] P. Appendini and J. H. Hotchkiss, *Innov. Food Sci. Emerg. Technol*., **3**, 113 (2002).
[8] L. A. Terry, S. F. White and L. J. Tigwell, *J. Agric. Food Chem*., **53**, 1309 (2005).
[9] J. Weiss, P. Takhistov and D. J. McClements, *J. Food Sci*., **71**, 107 (2006).
[10] A. Rahmani-Sani, A. Hosseini-Bandegharaei, S. H. Hosseini, K. Kharghani, H. Zarei *et al*., *J. Hazard. Mater*., **286**, 152 (2015).
[11] C. M. Antonio-Cisneros, M. M. Dávila-Jiménez, M. P. Elizalde-González and E. García-Díaz, *Food Chem*., **173**, 725 (2015).
[12] A. P. Periasamy, Y. H. Ho and S. M. Chen, *Biosens. Bioelectron*., **29**, 151 (2011).
[13] P. B. Filson, B. E. Dawson-Andoh and D. Schwegler-Berry, *Green Chem*., **11**, 1808 (2009).
[14] S. Ahola, X. Turon, M. Osterberg, J. Laine and O. J. Rojas, *Langmuir*, **24**, 11592 (2008).
[15] P. R. Chang, R. Jian, P. Zheng, J. Yu and X. Ma, *Carbohyd. Polym*., **79**, 301 (2010).
[16] J. Zhang, T. J. Elder, Y. Pu and A. J. Ragauskas, *Carbohyd. Polym*., **69**, 607 (2007).
[17] S. Beck-Candanedo, M. Roman and D. G. Gray, *Biomacromolecules*, **6**, 1048 (2005).
[18] J. Han, C. Zhou, Y. Wu and F. Liu, *Biomacromolecules*, **14**, 1529 (2013).
[19] I. Scarpa and A. Beavins, Patent US5245024, 1993.
[20] R. Dash, T. Elder and A. J. Ragauskas, *Carbohyd. Polym*., **88**, 789 (2012).
[21] M. Ioelovich, *Tappi J*., **13**, 45 (2014).
[22] K. E. Yunusov, A. A. Sarymsakov and S.S. Rashidova, *Polym. Sci. A*, **56**, 283 (2014).
[23] J. D. Fernández-Quiroz, S. R. Vásquez-García, N. Flores-Ramirez, G. Luna-Barcenas and O. Gutiérrez-Arriag, *Rev. Latin Am. Metal. Mat. SI*, **3**, 1243 (2009).
[24] G. Odian, "Principles of Polymerization", 4th ed., Wiley Interscience, USA, 2004, pp. 745.
[25] M.-C. Popescu, C.-M. Popescu, G. Lisa and Y. Sakata, *J. Mol. Struct*., **988**, 65 (2011).